# A clinical microchip for evaluation of single immune cells reveals high functional heterogeneity in phenotypically similar T cells

**Chao Ma**[1,2,5], **Rong Fan**[1,2,4,5], **Habib Ahmad**[1,2], **Qihui Shi**[1,2], **Begonya Comin-Anduix**[3], **Thinle Chodon**[3], **Richard C Koya**[3], **Chao-Chao Liu**[2], **Gabriel A. Kwong**[1,2], **Caius G. Radu**[1,3], **Antoni Ribas**[1,3], and **James R. Heath**[1,2]

[1]NanoSystems Biology Cancer Center, California Institute of Technology, Pasadena, California, USA

[2]Division of Chemistry and Chemical Engineering, California Institute of Technology, Pasadena, California, USA

[3]David Geffen School of Medicine, University of California–Los Angeles (UCLA), Los Angeles, California, USA

## Abstract

Cellular immunity has an inherent high level of functional heterogeneity. Capturing the full spectrum of these functions requires analysis of large numbers of effector molecules from single cells. We report a microfluidic platform designed for highly multiplexed (more than ten proteins), reliable, sample-efficient (~$1 \times 10^4$ cells) and quantitative measurements of secreted proteins from single cells. We validated the platform by assessment of multiple inflammatory cytokines from lipopolysaccharide (LPS)-stimulated human macrophages and comparison to standard immunotechnologies. We applied the platform toward the *ex vivo* quantification of T cell polyfunctional diversity via the simultaneous measurement of a dozen effector molecules secreted from tumor antigen–specific cytotoxic T lymphocytes (CTLs) that were actively responding to tumor and compared against a cohort of healthy donor controls. We observed profound, yet focused, functional heterogeneity in active tumor antigen–specific CTLs, with the major functional phenotypes quantitatively identified. The platform represents a new and informative tool for immune monitoring and clinical assessment.

In response to infection or tissue dysfunction, immune cells develop into highly heterogeneous repertoires with diverse functions[1–8]. A homeostatic makeup of these functional phenotypes dictates the overarching effect of an immune response[4,9,10]. For

example, tumor-infiltrating macrophages are activated to be either proinflammatory or regulatory depending on their interactions with other cells within the local microenvironment[11–14]. Viral infection leads to activated T cells with a large variety of effector functions, as reflected by different cytokine profiles[15,16]. Thus, a comprehensive characterization of the multifunctional phenotypes of single immune cells could provide both fundamental immunobiological information and clinically relevant data[5,17].

Common techniques for single-cell protein assays include enzyme-linked immunosorbent spot (Fluorospot) and intracellular cytokine staining (ICS) flow cytometry[6]. For enzyme-linked immunosorbent spot assays, typically one to three secreted proteins are detected at the single-cell level. The approach can be quantitative for detecting cytokine-secreting cells, but it does not quantify amounts of the secreted proteins. ICS flow cytometry has enabled the detection of up to five cytokines from single cells. Measurements of polyfunctionality may provide a better indication of *in vivo* activity, relative to phenotypic classifications based on cell surface markers[4]. This implies the need for measurements of increasing numbers of functions, via multiplex protein assays, from single cells.

Here we report on the single-cell barcode chip (SCBC) for the high-content assessment of functional heterogeneity at the single-cell level. The chip is comprised of 1,040 3-nl volume microchambers, each loaded with single cells or small defined numbers of cells. Protein concentrations are measured with immunosandwich assays from a spatially encoded antibody barcode. A full barcode represents a complete panel of protein assays, and duplicate barcodes per microchamber enable measurement statistics at the single-cell level. The SCBC permits on-chip, highly multiplexed detection of subthousand copies of proteins and requires only $\sim 1 \times 10^4$ cells to perform the assay.

We validated the technique with a human macrophage cell line to demonstrate detection of multiple cytokines from single cells. We then implemented it to assay the polyfunctionality of tumor antigen–specific T cells in the setting of an adoptive cell transfer (ACT) therapy clinical trial for melanoma. We observed focused, yet highly heterogeneous, functional diversity compared to samples from healthy donor controls. The SCBC is a high-throughput, low-cost and portable platform that can be used in a wide range of fundamental and clinical applications.

## RESULTS

### Design rationale and detection limit of the SCBC

The SCBC system consists of four modules (Fig. 1): microchannels that contain cells, control valves that isolate cells into microchambers, inlet and outlet ports for the introduction and depletion of reagents and cells and a barcode-encoded glass substrate for protein detection. The chip itself consists of two polydimethylsiloxane (PDMS) layers and fits onto a microscope slide (Fig. 1a). The bottom PDMS layer has inlets for the loading of reagents and cells that branch into 80 microchannels of $100~\mu m \times 17~\mu m$ cross-sectional size. Thirteen sets of vertical valves on the top PDMS layer divide those microchannels into 1,040-nl–volume microchambers. For a microchamber containing one to ten cells, the cell density is $0.3 \times 10^6$–$3 \times 10^6$ cells ml$^{-1}$, falling into the normal range for culture conditions and physiological environments[18].

The barcode array is a pattern of parallel stripes, each coated with a distinctive antibody. The stripe width is $25~\mu m$ at a pitch of $50~\mu m$. To achieve high and consistent antibody loading, and to prevent antibody denaturation during microfluidics assembly, we used the DNA-encoded antibody library (DEAL) approach[18], coupled with microchannel-guided flow patterning[19] (Supplementary Fig. 1). The chemistry and reproducibility of the DNA

barcode patterning process has been previously described[19–21]. The SCBC bar-codes contain 13 stripes, 12 for assaying a dozen different proteins and one as a control and spatial reference. Two sets of barcodes are included per microchamber. Cells are randomly loaded so that each SCBC microchamber contains zero to a few cells, following a amma Poisson distribution (goodness-of-fit test: $P > 0.8$. Supplementary Fig. 2). The numbers of cells in each chamber are counted via imaging (Fig. 1b).

We determined the dynamic range and detection limit of our design by performing on-chip immunoassays with recombinant proteins (Fig. 1c). The barcode array initially consists of 13 uniquely designed orthogonal DNA strands labeled in order as A through M (Supplementary Table 1). Before loading of recombinant proteins, a cocktail containing all capture antibodies conjugated to different complementary DNA strands (A′—L′) is used to transform, via DNA hybridization, the DNA barcode into an antibody array (Fig. 1c). As few as 100–1,000 copies ($1 \times 10^{-22}$–$1 \times 10^{-21}$ mol) could be detected (3 s.d.), with a dynamic range of three to four orders of magnitude (Fig. 1e and Supplementary Fig. 3), which is compatible with single-cell secretion measurements[18]. Antibody loading, and thus assay sensitivity, was uniform across the whole chip (coefficient of variation (CV) <10%) (Fig. 1d,e).

## Analysis of cytokine production by LPS-stimulated macrophages

We validated the SCBC by using the THP-1 human monocyte cell line. We differentiated the THP-1 cells into cytokine-producing macrophages using phorbol 12-myristate 13-acetate (PMA). Before loading into the device, we added LPS to activate Toll-like receptor 4 (TLR4) signaling[22,23], a process that mimics the innate immune response to Gram-negative bacteria (Supplementary Fig. 4). For these experiments, we designed the antibody barcode to measure 12 proteins: tumor necrosis factor-α (TNF-α), interferon-γ (IFN-γ), interleukin-2 (IL-2), IL-1α, IL-1β, IL-6, IL-10, IL-12, granulocyte-macrophage colony–stimulating factor (GM-CSF), chemokine (C-C motif) ligand-2 (CCL-2), transforming growth factor-β (TGF-β) and prostate-specific antigen (PSA) (Supplementary Table 2).

The microchambers contained between 0 and 40 cells so that both single-cell behavior and signals from a population could be measured. Through an automated image processing algorithm, we quantified the fluorescence intensities for each protein from each microchamber. For chambers with cells centered between the two barcodes, measurements from the barcode replicates were consistent (CV < 15%, Fig. 2). Uncentered cells contributed to variance between replicates (CV up to 50%); however, the averages of the barcode replicates from chambers with centered and uncentered cells were indistinguishable ($P > 0.2$, Supplementary Fig. 5). Furthermore, measurements between chips showed good consistency ($P > 0.2$).

The intensities of the individual proteins, averaged over many individual SCBC microchamber measurements, agreed with measurements of those same proteins from cell culture supernatants (Fig. 2a). Secretome data, when binned according to the numbers of cells per chamber, yielded statistically distinct protein signals ($P < 0.05$, Fig. 2b and Supplementary Fig. 6). However, the reference signal was insensitive to the numbers of cells ($P > 0.2$, Fig. 2b and Supplementary Fig. 6). Most notably, single-cell protein signals could be clearly detected ($P < 0.0001$, Fig. 2b and Supplementary Fig. 6). There was also clear separation of secreting and nonsecreting cells, as visualized by multiple peaks in flow cytometry histograms (Fig. 2c).

We gated the fraction of cells detected to secrete a given protein using background signals from empty chambers. We measured the frequencies of cells producing TNF-α, IL-1β, IL-10 and GM-CSF to be similar by both SCBC and by ICS flow cytometry (Fig. 2c and

Supplementary Fig. 6). Furthermore, the measured fraction of cells in each quadrant also showed a good similarity between the two techniques (Fig. 2c and Supplementary Fig. 6). Thus, the SCBC platform can efficiently provide a functional profiling of single immune cells. In general, these macrophages showed strongly coordinated functions[24].

## Analysis of polycytokine production by human CTLs

We next turned toward using the SCBC to functionally profile antigen-specific CTLs, which are the main effector cell type of an adaptive immune response targeting intracellular pathogens[25]. CTLs can show a great diversity of antigen specificities, phenotypic surface proteins and functions, and capturing this diversity is a major challenge. Most data suggest that the ability of CTLs to produce multiple cytokines (polyfunctionality) correlates with protective immune responses *in vivo*[4,26,27].

We assayed the functional diversity of healthy donor CD8^{+} T cells ($n = 3$), melanoma-associated antigen recognized by T cells 1 (MART-1)–specific T cell receptor (TCR)-transgenic cells collected from the peripheral blood of an individual with metastatic melanoma participating in an ACT immunotherapy clinical trial, and *ex vivo*–expanded tyrosinase-specific T cells. TCR engineering provides a means to generate large quantities of antigen-specific T cells amenable to use for the therapy of cancer[28]. The TCR-transgenic cells collected from the peripheral blood had been previously generated *in vitro* by retroviral vector transduction to insert the two chains of a TCR specific for MART-1 and then expanded *ex vivo* for 2 d followed by re-infusion into the patient after a lymphodepletion conditioning regimen. The patient then received three vaccinations with dendritic cells pulsed with a MART-1 peptide and a high dose of IL-2 to further activate and expand the cells *in vivo*. Peripheral blood mononuclear cells (PBMCs) were collected on day 30 after re-infusion by leukapheresis, at a time when multiple metastatic melanoma lesions were responding to this therapy. The tyrosinase-specific T cell culture was generated *ex vivo* from a tyrosinase-specific cell culture obtained by peptide–human leukocyte antigen A0201 (HLA-A0201) tetramer–based selection followed by nonspecific expansion with CD3-specific antibody and IL-2 to obtain a population of nontransgenic but uniform antigen-specific T cells.

We enriched the PBMCs for CD3 marker by negative magnetic bead selection before sorting on DEAL-based CD8-specific antibody–coated or peptide–HLA-A0201 tetramer–coated microarrays[29]. Then we released CD3^{+}CD8^{+} or CD3^{+}tetramer^{+} cells from the micro-arrays. The released T cells underwent activation either by polyclonal TCR engagement of CD3 and CD28-specific antibody binding or by antigen-specific TCR engagement via tetramer and CD28-specific antibody. Activation and SCBC loading was completed within 5 min. To maximize the on-percentage of single-cell measurement to 25–40%, we loaded $\sim 1 \times 10^4$ sorted T cells in 5 μl medium into the device. Protein heat maps and plots that compare and contrast these different T cell groups are presented in Figure 3. We included multiple markers that indicate functions such as cytoxicity (perforin), T cell growth and differentiation (IL-2), apoptosis promotion (TNF-α and IFN-γ), inflammation (IL-1β, IL-6 and TNF-β), anti-inflammation (IL-10) and the stimulation and recruitment of other immune compartments (CCL-2, CCL-3CCL-5 and GM-CSF)[27] (Supplementary Table 3).

More than 20% (median) of the healthy donor CD3^{+}CD8^{+} T cells produced TNF-α, IL-6 and the chemokines CCL-2, CCL-3 and CCL-5. The MART-1–specific TCR–transgenic cells that were inducing an objective tumor response *in vivo* showed a wide range of positive functions demonstrated by the release of perforin, IL-1β, IL-10, IFN-γ, IL-2 and CCL-5 upon *ex vivo* antigen re-stimulation with the MART-1–HLA-A0201 tetramer. The functionality of the antigen-specific TCR-transgenic cells derived from the subject with melanoma was higher compared to the healthy donor lymphocytes in terms of both signal

intensity and fraction of positive cells (Fig. 3a,b,e). The frequency of cytokine-producing cells among the subject-derived TCR transgenic cells was consistent with Fluorospot results (Fig. 3d). Phenotyping results identified by flow cytometry of surface markers of T cell phenotype (Fig. 3c) illustrated that the population of subject-derived TCR-transgenic, MART-1–specific cells was mostly homogeneous; the principal (>90%) population of these cells was $CD8^+$ and had a phenotype consistent with effector $CCR7^-CD45RA^+$ T cells at a late differentiation stage (Fig. 3c)[15]. In comparison, the *ex vivo*–expanded tyrosinase-specific T cells showed decreased production of CCL-3, IL-6 and TNF-α (Fig. 3e). Consistent with the notion that *ex vivo* expansion of T cells by IL-2 and CD3-specific antibody results in terminal differentiation of T cells, the tyrosinase-specific T cell clone had elevated release of perforin, IL-1β and IL-2, compared to healthy control samples, upon activation (Fig. 3e and Supplementary Fig. 7).

### Evaluation of polyfunctionality

We analyzed the multivariate features of these T cell populations by studying the protein-protein correlations for two and three proteins. Pseudo–three-dimensional plots (Fig. 4a–c) of markers representing various functions revealed that certain functions of the MART-1–specific cell population were highly coordinated compared to the healthy donor cells. For example, 70% of $IL-6^+$ cells produced CCL-5, whereas for CTLs from healthy donors the frequency was around 50%. TNF-α and IFN-γ production were anticorrelated in MART-1–specific cells (Fig. 4c), with >90% of the population expressing at most one of these effector molecules. However, for the small fraction of MART-1– specific TCR–transgenic cells that were $TNF-α^+IFN-γ^+$, secretion of IL-2 was often an additional function (75%, Fig. 4). A full set of protein-protein correlations is provided in Supplementary Figure 8.

We defined functional subsets of the various T cells by identifying groups of cells that secreted the same combination of proteins (Fig. 4d,e). There were at least 45 distinct subpopulations that accounted for 60% of the MART-1–specific TCR–transgenic cells (Fig. 4e and Table 1). A similar accounting for the healthy donor $CD8^+$ T cells and the tyrosinase-specific T cells yields 4–17 subpopulations (Fig. 4d and Table 1). Furthermore, for the MART-1–specific TCR–transgenic cells, the major functional subsets averaged more than five active functions, whereas both healthy donor and tyrosinase-specific cells averaged only one or two functions (Table 1). This demonstrates the ability of SCBC to visualize and discriminate different levels of functional heterogeneity.

## DISCUSSION

The SCBC permits highly multiplexed (more than ten proteins) measurements of effector molecules from single cells by detecting the natural protein secretome from macrophages and T cells upon activation. The multiplex capacity can be further expanded beyond what we explored here. The ability to use small sample size (~$1 \times 10^4$ cells) implies that the SCBC can be integrated with other upstream multiplexed analysis, such as flow cytometry or (as we show here) microarray sorting, to enable a detailed functional study of phenotypically defined sets of cells selected from heterogeneous populations. Analysis of signals from chambers containing different numbers of cells may also provide information relevant to cell-cell interactions.

The MART-1–specific TCR–transgenic CTLs had stronger perforin, IFN-γ and interleukin secretion and more functional heterogeneity compared with the healthy donor CTL controls. This functional status is also indicated by their identity as effector T cells ($CD45RA^+CCL7^-CD27^-CD28^-CD62L^-$)[15,30,31]. Previous vaccination studies identified that polyfunctional T cells are better cytokine producers and that the quality of a polyfunctional T cell response is a good predictor of clinical outcome[4,32]. We found that the

MART-1–specific TCR–transgenic CTLs showed favorable features compared against CTLs from healthy donors (for example, polyfunctional subset frequency 62% versus 6–25%; Supplementary Fig. 9). These data are consistent with the observation that, at the time the CTLs were collected, there was active inflammation and the tumors were responding to the ACT therapy in this patient.

We observed signs of T cell terminal effector differentiation and exhaustion, as indicated by the anticorrelation of TNF-α and IFN-γ secretion, high IL-10^{+} cell frequency and high PD1 and CD127 expression[15]. However, the quality of the T cell response at a single time point within a vaccination trial may not provide an indicator of long-term vaccination or therapy response[4]. A similar multiparameter SCBC analysis carried out at multiple time points throughout the course of a cancer immunotherapy treatment is currently underway.

We saw a high level of functional heterogeneity within a population defined as relatively homogeneous by surface markers[25,33], and that heterogeneity was also focused. For example, 45 out of >4,000 possible functional subsets could account for 60% of all MART-1–specific TCR-transgenic cells. The observed high level of polyfunctionality (up to 12 functions per cell, with an average of more than five functions) exceeds current multiplexing capacity by most existing single-cell secretion assays. Moreover, none of the proteins being profiled were interchangeable with others within the panel (with $R^2 < 0.6$, Supplementary Fig. 8). These findings indicate that a high dimensional analysis is in fact required for comprehensively profiling of T cell effector functions.

The SCBC provides a new platform for analyzing the functional activity of immune cells immediately after short-term *ex vivo* activation. This technology compares favorably to current cellular immunoassays in terms of sensitivity, multiplexing capacity, quantification, sample size, cost and infrastructure requirements and thus has potential for a thorough, cost-effective characterization of human immune cell responses.

# ONLINE METHODS

## Microchip fabrication

The SCBCs were assembled from a DNA barcode microarray glass slide and a PDMS slab containing a microfluidic circuit. The DNA barcode array was created with microchannel-guided flow patterning (Supplementary Fig. 1). Each barcode was comprised of thirteen stripes of uniquely designed single-stranded DNA molecules. The PDMS microfluidic chip was fabricated using a two-layer soft lithography approach[34] (Supplementary Methods).

## Human samples

Human samples were obtained from individuals with meta-static melanoma (males) enrolled in a TCR-transgenic ACT protocol clinical trial (registration number NCT00910650). The studies using human samples were approved by the appropriate human use committees (UCLA Institutional Review Board 08-02-020, IND# 13859), and informed consent was obtained from all individuals studied.

## Isolation, purification and expansion of T cells

PBMCs were collected from individuals receiving TCR ACT immunotherapy by leukapheresis and periodic peripheral blood draws as previously described[35]. Aliquots of cryopreserved PBMCs were thawed and immediately diluted with RPMI complete medium containing 5% human AB serum (Omega Scientific). Cells were washed and subjected to enzymatic treatment with DNase (Sigma) for 1 h at 37 °C, washed and rested overnight in a 5% $CO_2$ incubator. Antigen-specific MART-1 T cells were purified sequentially by

magnetic negative enrichment for CD3 (Stemcell) and by a MART-1–HLA-A0201 tetramer microarray that have been previously described[29] (Supplementary Methods). Purified cells were collected, washed, stimulated with MART-1 tetramer and CD28-specific antibody and loaded into SCBC chip. PBMCs from healthy donors were negatively enriched in the same way and were further purified by CD8-specific antibody microarray, followed by stimulation with CD3/CD28–specific antibody. Sorted cells was checked to be >95% pure.

### On-chip secretion profiling

Before loading cells onto the chip, the DNA barcode array was transformed into an antibody microarray. The chip was then ready for cell loading. Chips with cells were incubated and then assays were developed with secondary antibodies and fluorescent markers (Supplementary Methods).

### Intracellular cytokine staining of THP-1 cells

Brefeldin A (eBioscience) was added in the presence of PMA and LPS at the recommended concentration in the final 4 h of stimulation. Standard intracellular staining was performed as described by the supplier's protocol (eBioscience) with additional blocking with human serum (Sigma) and washes. Cells were fixed and permeabilized by using a fixation and permeabilization kit (eBioscience) and then were stained intracellularly with antibody to TNF-α (MAb11), antibody to IL-1β (H1b-98), antibody to IL-10 (JES3-9D7) and antibody to GM-CSF (BVD2-21C11) (all from eBioscience). Isotype control staining was used as negative control, and $2 \times 10^4$ events were collected for each condition. Samples were analyzed on a FACSCalibur (BD Biosciences) machine with CellQuest Pro software (BD Biosciences).

### Flow cytometry analysis of antigen specific T cells

Cryopreserved PBMC samples from peripheral blood draws or leukapheresis were thawed and analyzed by HLA-A*0201 tetramer assay (Beckman Coulter) with flow cytometric analysis as previously described[35,36]. In brief, PBMCs were resuspended in 100 μl of adult bovine serum (Omega Scientific) and stained for 15 min at room temperature (20 °C) using a cocktail of antibodies to the following proteins in replicate aliquots: CD3 (UCHT1, BD Bioscience), CD8 (3B5, Invitrogen), CD45RA (2H4LDHIILDB9, Beckman Coulter), CD62L (DREG56, Beckman Coulter), CCR7 (150503, BD Bioscience), CD27 (MT271, BD Bioscience), CD28 (CD28.2, BD Bioscience), CD127 (HIL-7R-M21, BD Bioscience) and PD1 (MIH4, BD Bioscience). For all flow cytometry experiments, anti-mouse IgK isotype control FBS compensation particles (BD Biosciences) were used for compensation purposes, and $5 \times 10^5$ to $1 \times 10^6$ lymphocytes were acquired for each condition. To correctly gate the flow cytometry data, the fluorescent minus one approach was used. Samples were acquired on an LSR II system (BD Biosciences), and data were analyzed using FlowJo software (TreeStar).

### Fluorospot assay for sorted antigen-specific T cells

Antigen specific T cells were captured by tetramer microarray. Primary cytokine capture antibody was co-localized on the same array. The captured cells were then incubated at 37 °C and 5% $CO_2$ for 12 h in 10% FBS in RPMI 1640 medium. Phycoerythrin-labeled secondary antibody (eBioscience) was applied after incubation. Then slides were washed and imaged by the EZ-C1 confocal microscope system (Nikon).

### Data and statistical analyses

We used GenePix 4400 (Axon Instruments) to obtain the scanned fluorescent image for both Cy3 and Cy5 channels. All scans were performed at constant instrument settings: laser

power 80% (635 nm) and 15% (532 nm), optical gains 600 (635 nm) and 450 (532 nm), brightness 80 and contrast 83 for T cell experiments; laser power 100% (635 nm) and 33% (532 nm), optical gains 800 (635 nm) and 700 (532 nm), brightness 87 and contrast 88 for macrophage experiments. All the barcodes were processed in PhotoShop (Adobe) and ImageJ software (US National Institutes of Health) to generate fluorescence line profiles. A home-developed Excel (MicroSoft) macro was employed for automatic extraction of average fluorescence signal for all bars in each set of barcode, and all the barcode profiles were compared to the number of cells by using the same program. On the basis of these data, heat maps were generated by using the software Cluster and Treeview[37]. Flow cytometry data were analyzed in FlowJo software. *P* values were calculated from two-tailed Student's *t* tests assuming unequal variance.

### Additional methods

Detailed methodology is described in the Supplementary Methods.

## Supplementary Material

Refer to Web version on PubMed Central for supplementary material.

## Acknowledgments

## References

1. Gordon S, Taylor PR. Monocyte and macrophage heterogeneity. Nat Rev Immunol. 2005; 5:953–964. [PubMed: 16322748]

2. O'Shea JJ, Hunter CA, Germain RN. T cell heterogeneity: firmly fixed, predominantly plastic or merely malleable? Nat Immunol. 2008; 9:450–453. [PubMed: 18425095]

3. Kaech SM, Wherry EJ. Heterogeneity and cell-fate decisions in effector and memory CD8$^+$ T cell differentiation during viral infection. Immunity. 2007; 27:393–405. [PubMed: 17892848]

4. Darrah PA, et al. Multifunctional T$_H$1 cells define a correlate of vaccine-mediated protection against *Leishmania major*. Nat Med. 2007; 13:843–850. [PubMed: 17558415]

5. Lee PP, et al. Characterization of circulating T cells specific for tumor-associated antigens in melanoma patients. Nat Med. 1999; 5:677–685. [PubMed: 10371507]

6. Seder RA, Darrah PA, Roederer M. T-cell quality in memory and protection: implications for vaccine design. Nat Rev Immunol. 2008; 8:247–258. [PubMed: 18323851]

7. Re F, Strominger JL. Heterogeneity of TLR-induced responses in dendritic cells: from innate to adaptive immunity. Immunobiology. 2004; 209:191–198. [PubMed: 15481153]

8. Chattopadhyay PK, Yu J, Roederer M. A live-cell assay to detect antigen-specific CD4+ T cells with diverse cytokine profiles. Nat Med. 2005; 11:1113–1117. [PubMed: 16186817]

9. Zak DE, Aderem A. Systems biology of innate immunity. Immunol Rev. 2009; 227:264–282. [PubMed: 19120490]

10. Precopio ML, et al. Immunization with vaccinia virus induces polyfunctional and phenotypically distinctive CD8$^+$ T cell responses. J Exp Med. 2007; 204:1405–1416. [PubMed: 17535971]

11. Mantovani A, Allavena P, Sica A, Balkwill F. Cancer-related inflammation. Nature. 2008; 454:436–444. [PubMed: 18650914]

12. Coussens LM, Werb Z. Inflammation and cancer. Nature. 2002; 420:860–867. [PubMed: 12490959]

13. Medzhitov R. Origin and physiological roles of inflammation. Nature. 2008; 454:428–435. [PubMed: 18650913]

14. Hagemann T, Balkwill F, Lawrence T. Inflammation and cancer: a double-edged sword. Cancer Cell. 2007; 12:300–301. [PubMed: 17936555]

15. Appay V, van Lier RAW, Sallusto F, Roederer M. Phenotype and function of human T lymphocyte subsets: consensus and issues. Cytometry A. 2008; 73:975–983. [PubMed: 18785267]

16. Song K, et al. Characterization of subsets of CD4+ memory T cells reveals early branched pathways of T cell differentiation in humans. Proc Natl Acad Sci USA. 2005; 102:7916–7921. [PubMed: 15905333]

17. Kotecha N, et al. Single-cell profiling identifies aberrant STAT5 activation in myeloid malignancies with specific clinical and biologic correlates. Cancer Cell. 2008; 14:335–343. [PubMed: 18835035]

18. Bailey RC, Kwong GA, Radu CG, Witte ON, Heath JR. DNA-encoded antibody libraries: A unified platform for multiplexed cell sorting and detection of genes and proteins. J Am Chem Soc. 2007; 129:1959–1967. [PubMed: 17260987]

19. Fan R, et al. Integrated barcode chips for rapid, multiplexed analysis of proteins in microliter quantities of blood. Nat Biotechnol. 2008; 26:1373–1378. [PubMed: 19029914]

20. Shin YS, et al. Chemistries for patterning robust DNA microbarcodes enable multiplex assays of cytoplasm proteins from single cancer cells. Chem Phys Chem. 2010; 11:3063–3069. [PubMed: 20715281]

21. Wang J, et al. A self-powered, one-step chip for rapid, quantitative and multiplexed detection of proteins from pinpricks of whole blood. Lab Chip. 2010; 10:3157–3162. [PubMed: 20924527]

22. Aderem A, Ulevitch RJ. Toll-like receptors in the induction of the innate immune response. Nature. 2000; 406:782–787. [PubMed: 10963608]

23. Fan J, Malik AB. Toll-like receptor 4 (TLR4) signaling augments chemokine-induced neutrophil migration by modulating cell surface expression of chemokine receptors. Nat Med. 2003; 9:315–321. [PubMed: 12592402]

24. Shin YS, et al. Protein signaling networks from single cell fluctuations and information theory profiling. Biophys J. (in the press).

25. Attig S, et al. Simultaneous Infiltration of polyfunctional effector and suppressor T cells into renal cell carcinomas. Cancer Res. 2009; 69:8412–8419. [PubMed: 19843860]

26. De Rosa SC, et al. Vaccination in humans generates broad T cell cytokine responses. J Immunol. 2004; 173:5372–5380. [PubMed: 15494483]

27. Makedonas G, Betts MR. Polyfunctional analysis of human t cell responses: importance in vaccine immunogenicity and natural infection. Springer Semin Immunopathol. 2006; 28:209–219. [PubMed: 16932955]

28. Morgan RA, et al. Cancer regression in patients after transfer of genetically engineered lymphocytes. Science. 2006; 314:126–129. [PubMed: 16946036]

29. Kwong GA, et al. Modular nucleic acid assembled p/MHC microarrays for multiplexed sorting of antigen-specific T cells. J Am Chem Soc. 2009; 131:9695–9703. [PubMed: 19552409]

30. Bachmann MF, Wolint P, Schwarz K, Jager P, Oxenius A. Functional properties and lineage relationship of CD8+ T cell subsets identified by expression of IL-7 receptorα and CD62L. J Immunol. 2005; 175:4686–4696. [PubMed: 16177116]

31. van Lier RAW, ten Berge IJM, Gamadia LE. Human CD8+ T-cell differentiation in response to viruses. Nat Rev Immunol. 2003; 3:931–939. [PubMed: 14647475]

32. Pantaleo G, Koup RA. Correlates of immune protection in HIV-1 infection: what we know, what we don't know, what we should know. Nat Med. 2004; 10:806–810. [PubMed: 15286782]

33. Ribas A, et al. Dendritic cell vaccination combined with CTLA4 blockade in patients with metastatic melanoma. Clin Cancer Res. 2009; 15:6267–6276. [PubMed: 19789309]

34. Thorsen T, Maerkl SJ, Quake SR. Microfluidic large-scale integration. Science. 2002; 298:580–584. [PubMed: 12351675]

35. Comin-Anduix B, et al. Detailed analysis of immunologic effects of the cytotoxic T lymphocyte-associated antigen 4–blocking monoclonal antibody tremelimumab in peripheral blood of patients with melanoma. J Transl Med. 2008; 6:22. [PubMed: 18452610]

36. Comin-Anduix B, et al. Definition of an immunologic response using the major histocompatibility complex tetramer and enzyme-linked immunospot assays. Clin Cancer Res. 2006; 12:107–116. [PubMed: 16397031]

37. Eisen MB, Spellman PT, Brown PO, Botstein D. Cluster analysis and display of genome-wide expression patterns. Proc Natl Acad Sci USA. 1998; 95:14863–14868. [PubMed: 9843981]
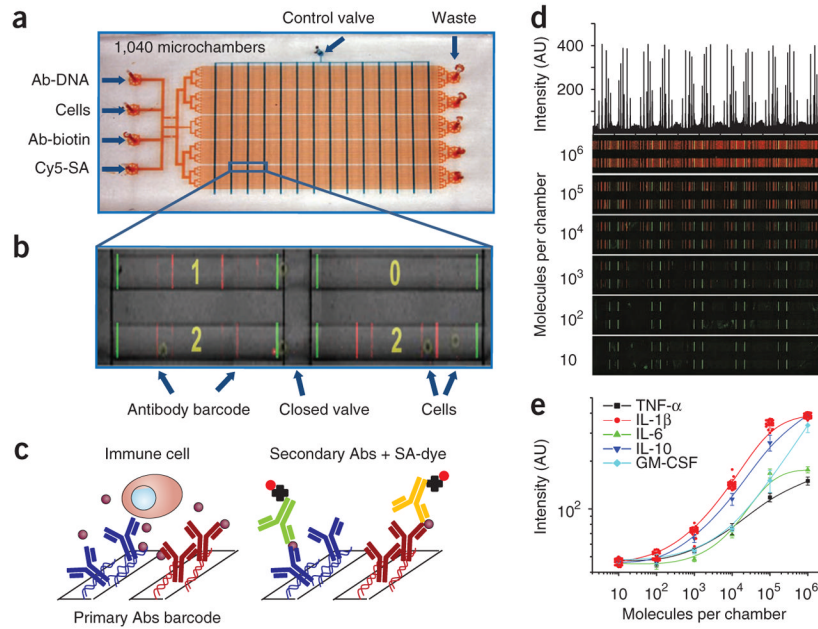
**Figure 1.**
Design of the SCBC for single-cell protein secretome analysis. (**a**) Image of an SCBC in which flow channels are shown in red and the control channels are shown in blue. Input and output ports are labeled. Ab, antibody. (**b**) An optical micrograph showing cells loaded and isolated within the microchambers, overlaid with the fluorescence micrograph of the developed assay barcode for those same microchambers. Numbers of cells per microchamber are indicated by the yellow numbers. (**c**) Drawing of the multiplex DEAL primary antibody barcode array used for capture of secreted proteins from single cells and then developed for the detection of those proteins. SA, Streptavidin. (**d**) Scanned fluorescent images used for the antibody barcode calibration measurements using spiked recombinant proteins. The protein concentrations (in numbers of molecules per chamber) are given to the left of each row of images. The plot at the top is a line profile of the top row of images and represents the reproducibility of the barcodes across the antibody array of an SCBC. (**e**) Recombinant protein calibration curves for TNF-α, IL-1β, IL-6, IL-10 and GM-CSF. Individual measurements (red) are shown for IL-1β. Other proteins measurements are represented by average intensity values and s.d.
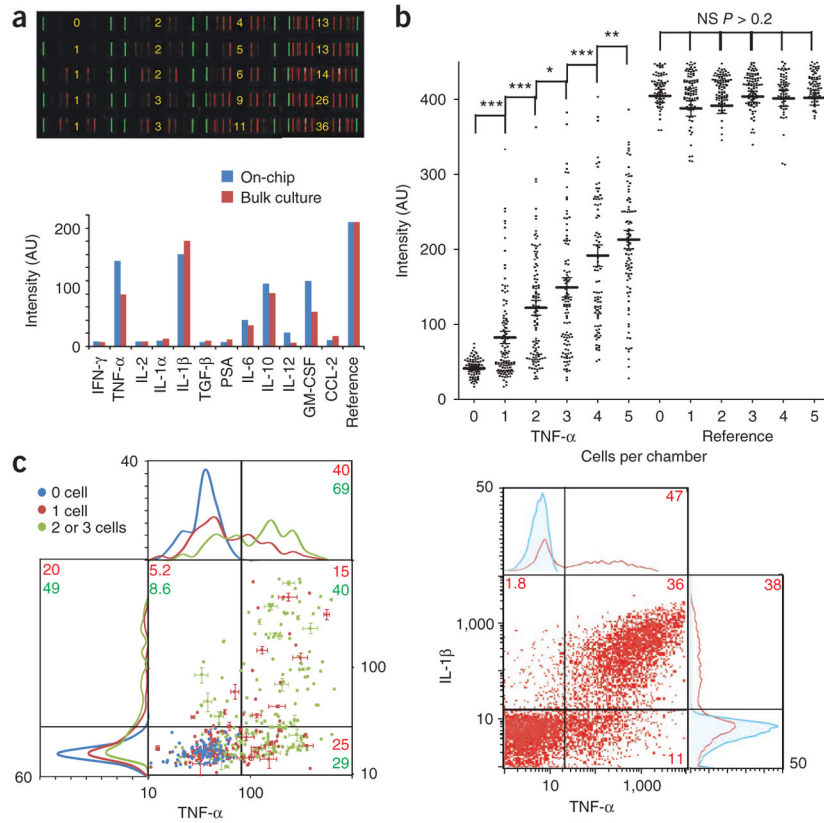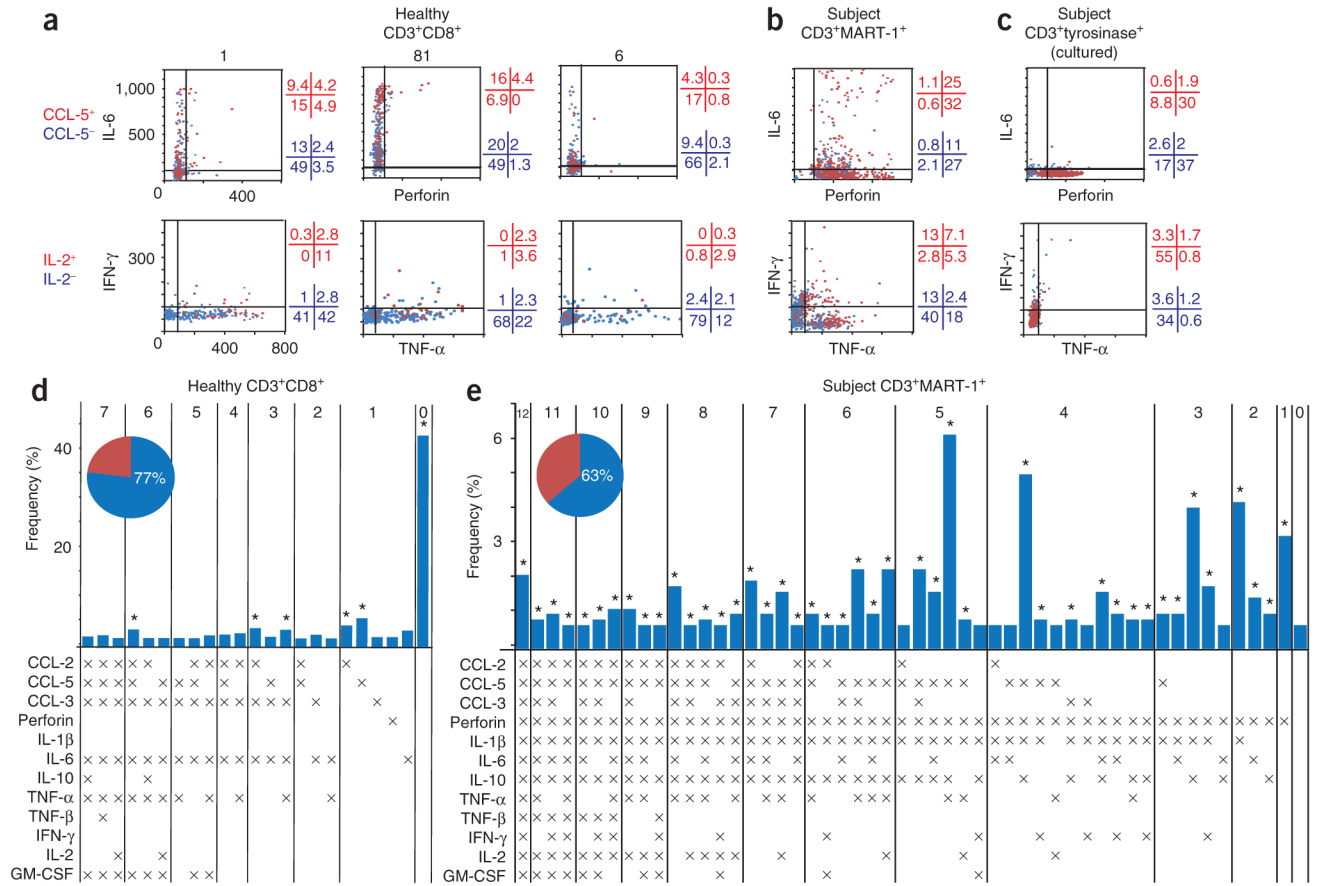
**Figure 2.**
On chip secretion measurements of macrophage differentiated from THP-1 monocyte cell.
(**a**) Top, representative scanned images of barcode signals from individual chambers. Green
bars represent microchamber boundaries, red bars are protein signals and the yellow
numbers indicate the number of cells. Bottom, comparison of averaged intensity from SCBC
measurements and bulk culture supernatant. Data are normalized so that references have the
same intensity. (**b**) Scatter plots of measured levels of TNF-α and the reference control for
individual microchambers containing $n = 0,1,2,3,4$ or 5 cells. $P$ values are calculated by
comparing neighboring columns (*$P < 0.005$; **$P < 0.001$; ***$P < 0.0001$; NS, not
significant). (**c**) Scatter plots of TNF-α versus IL-1β derived from SCBC measurements
(left) and from ICS coupled with flow cytometry (right). Histograms (frequency versus
intensity) for the individual protein are provided at the tops and sides of the scatter plots. All
$y$ axis units are fluorescence intensity. For the SCBC data, each quadrant is labeled with
numbers that reflect the percentage of single cells (red) and two to three cells (green) in that
section. The gates separating cytokine-secreting and nonsecreting cells are determined from
0 cell microchamber (background) measurements (blue). s.d. from barcode replicates of the
same chamber are provided for selected points (see Results for selection criteria). For the
ICS measurements, the gates were determined by isotype control staining.
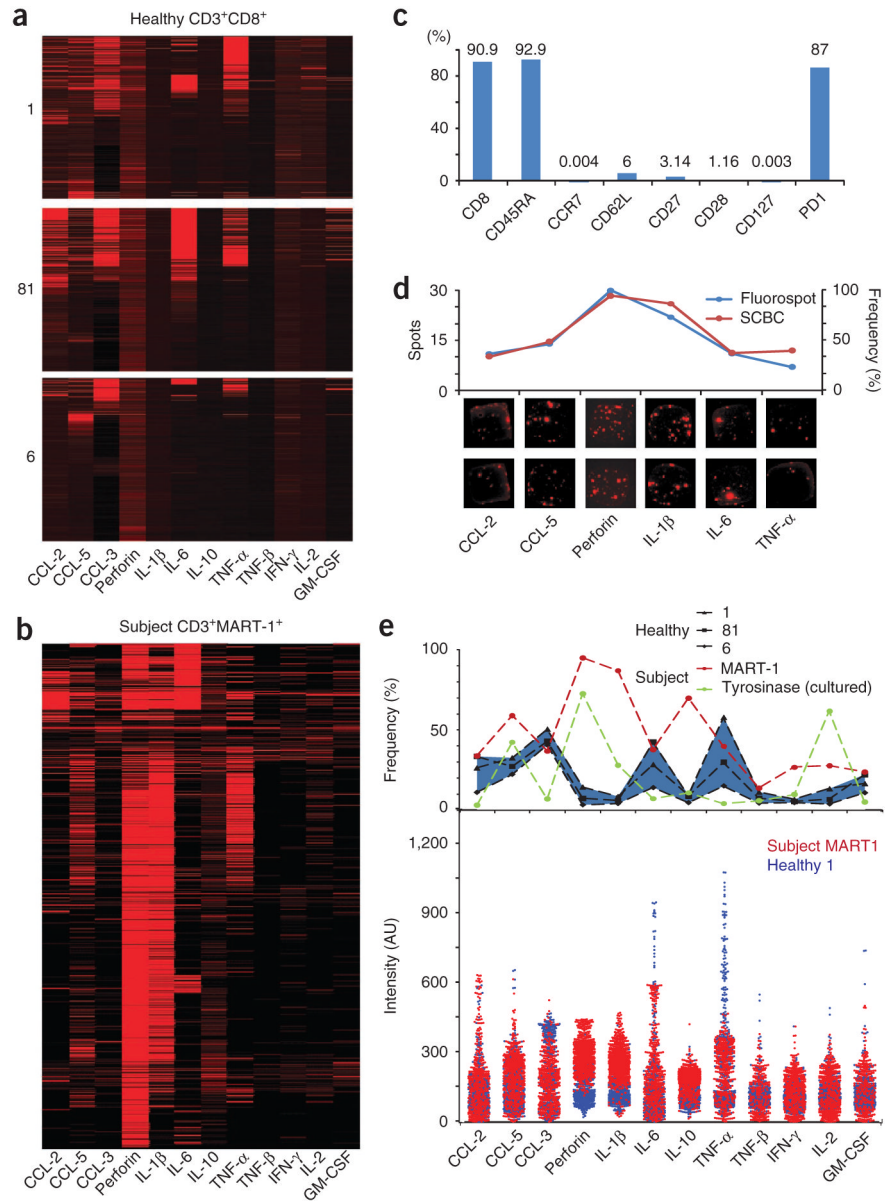
**Figure 3.**
Single-cell secretion measurements of CTLs from individuals with melanoma and healthy donors. (**a**) Unsupervised clustering of CD8+ T cells from three healthy donors, presented as a heat map. Each row represents a measurement of 12 secreted cytokines from a single cell, with protein labels provided at the bottom. (**b**) Data from MART-1–specific TCR–transgenic CTL single-cell experiments, presented as a heat map organized via unsupervised clustering. The fluorescence intensity scale for all four heat maps is the same. (**c**) Phenotyping data from flow cytometry for MART-1–specific TCR–transgenic CTLs. Each bar shows the percentage of cells positive for the specific surface marker. (**d**) Fluorospot analysis of the MART-1–specific TCR–transgenic T cell population. The curves on top compare SCBC and Fluorospot measurements on fraction (or number) of cells secreting CCL-2, CCL-5, perforin, IL-1β, IL-6 and TNF-α. Representative Fluorospot images are provided at the bottom. (**e**) Univariate comparison of antigen-specific TCR–transgenic T cells from a subject with melanoma and healthy donor CD8+ T cell culture controls. The

lines of the top plot represent the percentage of cytokine-producing cells from each sample. Blue area shows the range detected from healthy donor samples. The one-dimensional scatter plot on the bottom compares the signal intensities measured from the subject's MART-1–specific TCR–transgenic T cells and the CD8^{+} T cell background from one representative healthy donor.

**Figure 4.**
Polyfunctional diversity analysis for CTLs from a subject with metastatic melanoma and from healthy donors. (**a–c**) Pseudo–three-dimensional scatter plots for representative single-cell cytokine measurements from $CD8^+$ T cells. Top and bottom rows are correlations for perforin versus IL-6 and TNF-α versus IFN-γ, respectively. The third dimension (CCL-5 or IL-2) is projected to the two-dimensional plot by using red for positive cells and blue for negative cells. Numbers on the right show percentage in each quadrant. Samples are labeled on the left. (**d,e**) Functional diversity plots for the subject's MART-1–specific TCR–transgenic cells and $CD8^+$ T cells from a representative healthy donor. Each major functional subset identified (with frequency >0.5%) is shown by an individual bar. The bar heights represent population percentages. Fifty-three major subsets were identified from the MART-1–specific TCR–transgenic cells; 23 were identified from the healthy donor. The number at the top of the plot is the number of functions associated with each subset. The matrix at the bottom provides the function detail (×: positive). The pie charts give the percentage of cells that fell into one of the major functional subsets. Asterisks above the blue bars denote those subsets within the most frequent 60% of the population.

**Table 1**

Summary of functional diversity of assayed samples

| Sample | Major functional subsets identified | Percentage of total populations | Number of functions | | Functional subsets in top 60% populations | Number of functions | |
|---|---|---|---|---|---|---|---|
| | | | Range | Mean | | Range | Mean |
| Healthy CD3+ CD8+ | 1 | 70.3 | 0–7 | 1.68 | 17 | 0–5 | 1.32 |
| | 33 | | | | | | |
| | 81 | 77.4 | 0–7 | 1.44 | 6 | 0–6 | 1.34 |
| | 23 | | | | | | |
| | 6 | 80.2 | 0–7 | 0.89 | 4 | 0–2 | 0.36 |
| | 21 | | | | | | |
| Subject CD3+ MART1+ | 53 | 63.4 | 0–12 | 5.17 | 45 | 1–12 | 5.27 |
| Subject CD3+ tyrosinase+ (cultured) | 27 | 80.1 | 0–5 | 2.25 | 8 | 0–4 | 2.11 |